Supporting information

Fe_2O_3/ZnO heterojunction for efficient electrochemical nitrate reduction to ammonia

Huilin Zhao, Yun Duan, Xuetao Cheng, Chao Fan, and Yan-Qin Wang*

Inner Mongolia Key Laboratory of Chemistry and Physics of Rare Earth Materials, College of Chemistry and Chemical Engineering, Inner Mongolia University, Hohhot, 010021, China

E-mail: yqwang_chem@imu.edu.cn

Contents

1. Experimental Section

Electrochemical measurements of nitrate reduction reaction (NO_3RR)

Determination of ion concentration

The ultraviolet-visible (UV-Vis) spectrophotometer was applied to test the ion concentration of before and after-tested electrolytes after diluting to appropriate concentration to match the range of calibration curves. The specific test methods are as follows:

Determination of ammonia

The produced ammonia was determinate by salicylic acid-potassium sodium tartrate chromogenic reagent. First, the electrolyte after electrolysis was diluted to 2 mL by PBS, reaching the concentration range of detection. Then 2 mL of salicylate-potassium sodium tartrate color reagent was added into the diluted electrolyte and mixed thoroughly. 1 mL sodium hypochlorite and 0.2 mL sodium nitroprusside solution were added into the above solution. The absorption intensity at 655 nm was recorded by UV-Vis spectrophotometer after two hours of standing away from light. The concentration-absorbance curve was calibrated with a series of standard ammonium chloride solutions.

Determination of NO_3^-

First, the electrolyte after electrolysis was diluted to 2 mL, and 0.1 mL 1 M hydrochloric acid and 0.01 mL 0.8wt % sulfanilic acid solution were added to the diluted solution. After standing for 10 min, the absorption spectrum was measured by UV-visible spectrophotometer and the absorption intensity at 220 and 275 nm

wavelengths was recorded. The final absorbance is calculated as follows: $A = A_{220nm} - 2A_{275nm}$.The concentration-absorbance curve was calibrated with a series of standard potassium nitrate solutions.

Determination of NO_2^-

The chromogenic reagent was a mixture of p-aminobenzene sulfonamide (0.1 g), N-(1-naphthalene) ethylenediamine hydrochloride (0.01 g), deionized water (5 mL) and phosphoric acid (0.294 mL, ρ = 1.685 g mL^{-1}). First, the electrolytic solution was diluted to the detection concentration range, and then 1 mL color reagent was added. After shaking for 10 minutes, the absorbance at 540 nm was measured with an ultraviolet-visible spectrophotometer. The nitrite concentration was calculated using the calibration curve obtained.

Determination of N_2H_4

The coloring reagent was a mixture of anhydrous ethanol (50 mL), hydrochloric acid (5 mL) and p-$C_9H_{11}NO$ (1 g). First, a certain amount of electrolyte was diluted to 2 mL to reach the detection concentration range. 1 mL of color developing reagent was added to the above solution. After standing for 20 min, the absorption intensity at 455 nm was measured and recorded by UV-Vis spectrophotometer.

Isotope Labeling Experiments

In order to verify the source of ammonia, $K^{15}NO_3$ was used as the raw nitrogen source to carry out the isotope labeled nitrate reduction experiment. 0.1 M PBS and 0.1 M $K^{15}NO_3$ were used as the electrolyte. After electroreduction, 2 mL of the obtained $^{15}NH_4^+$ electrolyte was taken out, and the pH value of the electrolyte was

adjusted to weakly acidic with 1.0 M hydrochloric acid. Then 0.5 mL DMSO was added to 0.5 mL of the above mixed solution, and finally ^{1}H NMR (600 MHz) was used for qualitative analysis.

Quantitative detection of nitrogen.

N_2 generation from the cathodic compartment was analyzed using online gas 11 chromatography (GC 2060) equipped with a thermally conductive detector (TCD) and 12 a flammable ionization detector (FID).

The faradaic efficiency (FE) of N_2 was calculated by the following equation:

$$FE_{N2} = \frac{z * F * n}{Q} * 100\%$$

Where F is the Faraday constant, z is the number of transferred electrons, n is the mole number, and Q is the amount of the total charge passing through the system.

2. Computational Details

We have employed the first-principles[1,2] to perform density functional theory (DFT) calculations within the generalized gradient approximation (GGA) using the Perdew-Burke-Ernzerhof (PBE)[3] formulation. We have chosen the projected augmented wave (PAW) potentials[4-5] to describe the ionic cores and take valence electrons into account using a plane wave basis set with a kinetic energy cutoff of 520 eV. Partial occupancies of the Kohn-Sham orbitals were allowed using the Gaussian smearing method and a width of 0.05 eV. The electronic energy was considered self-consistent when the energy change was smaller than 10^{-5} eV. A geometry optimization was considered convergent when the force change was smaller than 0.05 eV Å^{-1}. The Brillouin zone integration is performed using 2 × 2 × 1 Monkhorst-Pack k-point sampling for a structure. Finally, the adsorption energies (Eads) were calculated as Eads = Ead/sub-Ead-Esub, where Ead/sub, Ead, and Esub are the total energies of the optimized adsorbate/substrate system, the adsorbate in the structure, and the clean

substrate, respectively. The free energy was calculated using the equation:

G = Eads + ZPE - TS

where G, Eads, ZPE and TS are the free energy, total energy from DFT calculations, zero-point energy and entropic contributions, respectively, where T is set to 300 K.

3. Supporting Figures and Tables

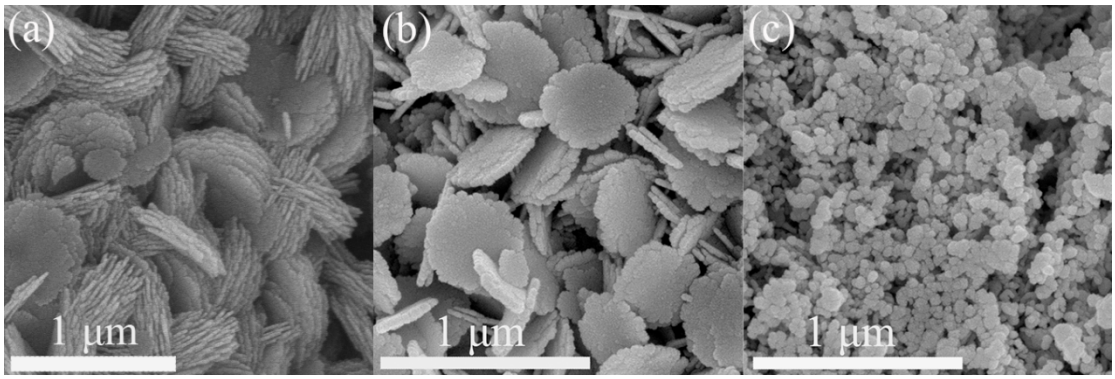

Fig. S1 (a) SEM images of Fe-MOF, (b) Fe_2O_3, (c) ZnO.

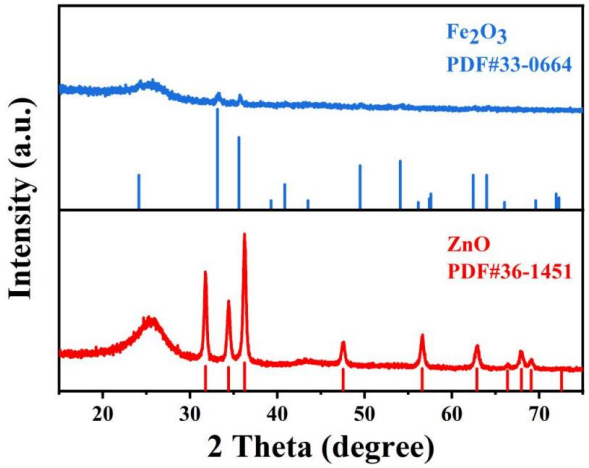

Fig. S2 The XRD patterns of Fe_2O_3 and ZnO.

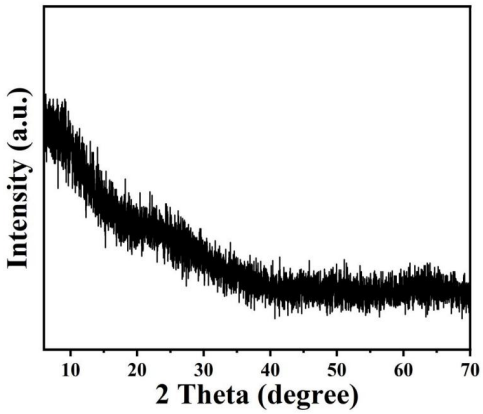

Fig. S3 The XRD pattern of Fe-MOF.

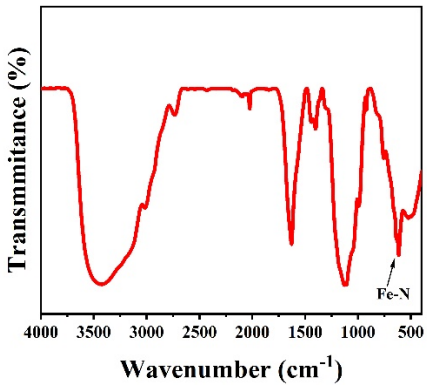

Fig. S4 The FTIR spectrum of Fe-MOF.

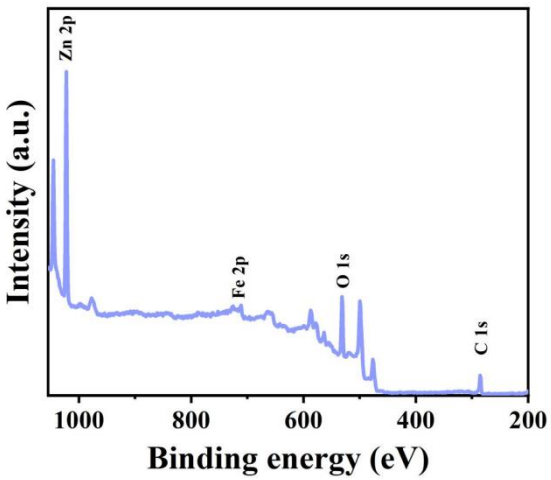

Fig. S5 The XPS survey spectra of Fe_2O_3/ZnO.

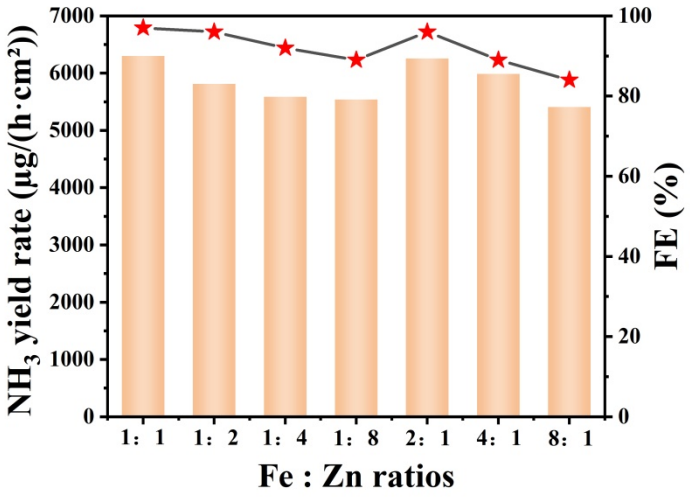

Fig. S6 The NH_3 yield and NH_3 Faraday efficiency of Fe_2O_3/ZnO with different Fe:Zn feed ratios at -1.0 V vs. RHE.

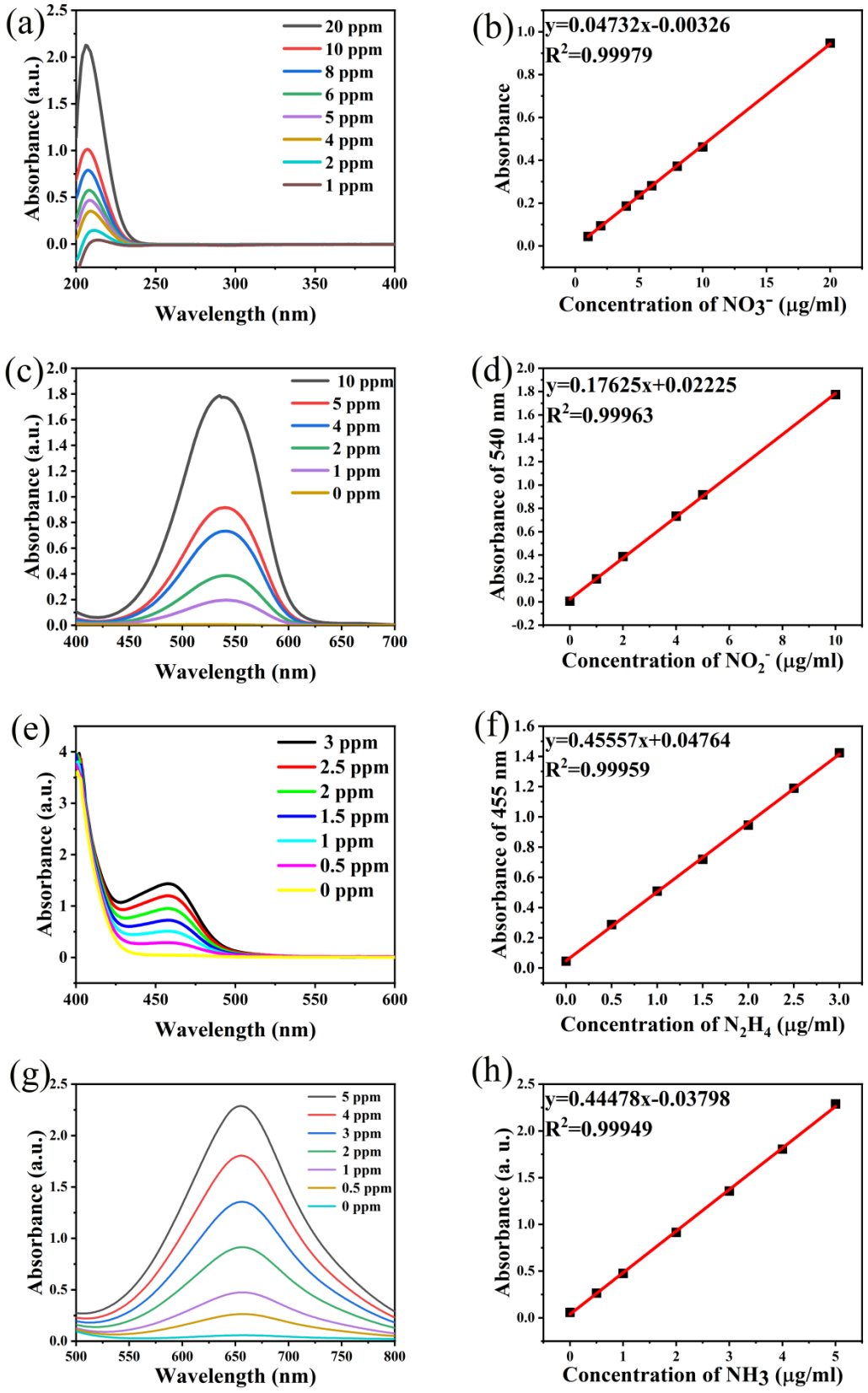

Fig. S7 (a) UV-Vis absorption spectroscopies for various concentrations of NO_3^--N. (b) Calibration curve used to estimate the concentration of NO_3^--N. (c) UV-Vis

absorption spectroscopies for various concentrations of NO_2^--N. (d) Calibration curve used to estimate the concentration of NO_2^--N. (e) UV-Vis absorption spectroscopies for various concentrations of N_2H_4. (f) Calibration curve used to estimate the concentration of N_2H_4. (g) UV-Vis absorption spectroscopies for various concentrations of NH_3. (h) Calibration curve used to estimate the concentration of NH_3.

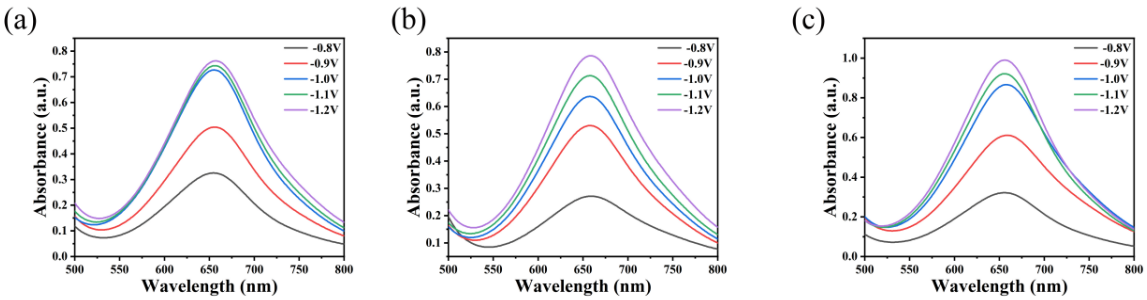

Fig. S8 The UV-vis spectra for (a) the first time (b) the second time and (c) the third time at five different potentials.

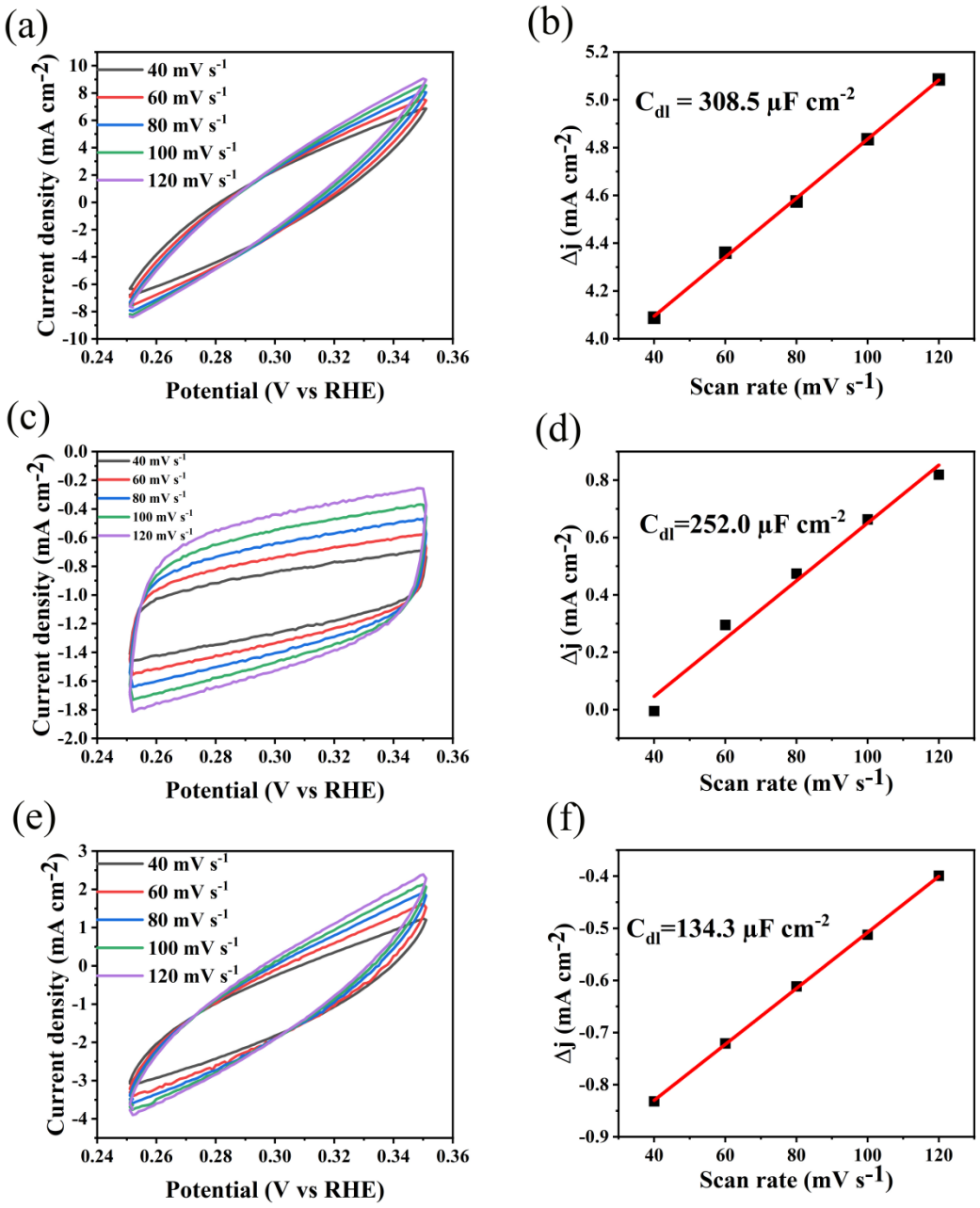

Fig. S9 (a) The CV curves at various scan rates and (b) capacitive current densities of the Fe_2O_3/ZnO. (c) The CV curves at various scan rates and (d) capacitive current densities of the Fe_2O_3. (e) The CV curves at various scan rates and (f) capacitive current densities of the ZnO.

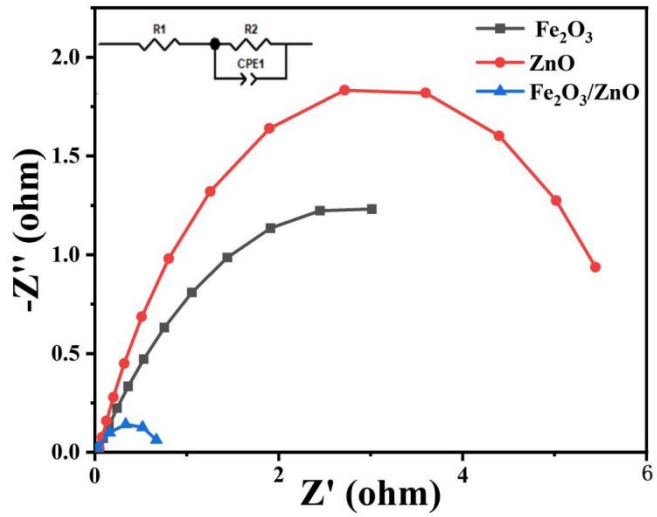

Fig. S10 Nyquist plots of Fe_2O_3/ZnO, Fe_2O_3 and ZnO at -1.0 V (vs. RHE) in 0.1 M PBS solution.

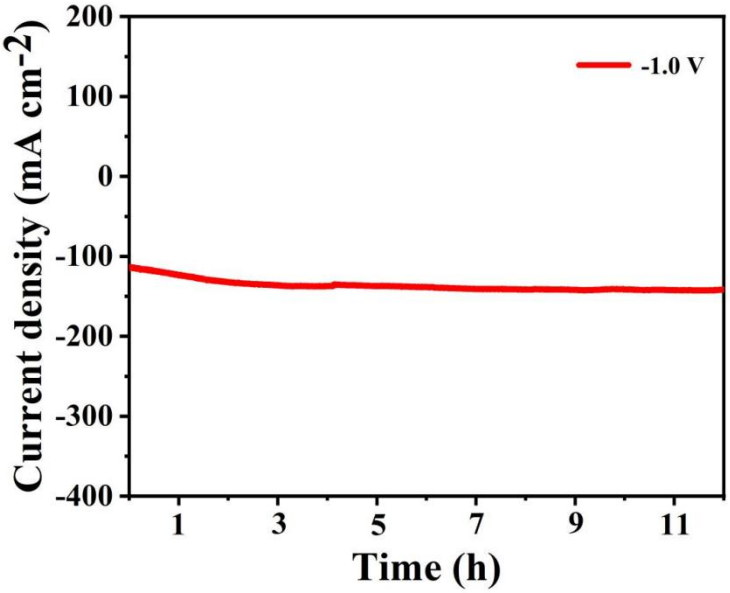

Fig. S11 The i-t curve of Fe_2O_3/ZnO tested continuously for 12 hours at -1.0 V (vs. RHE).

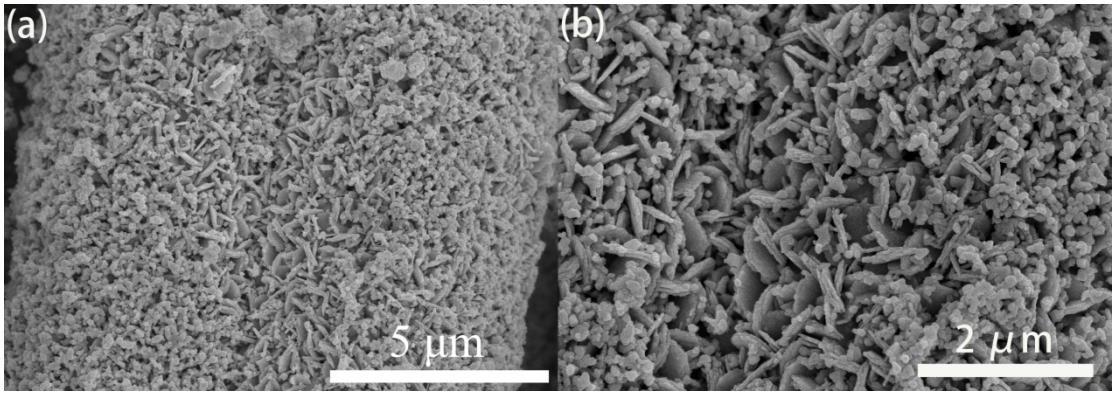

Fig. S12 (a-b) SEM images of Fe_2O_3/ZnO after NO_3RR test.

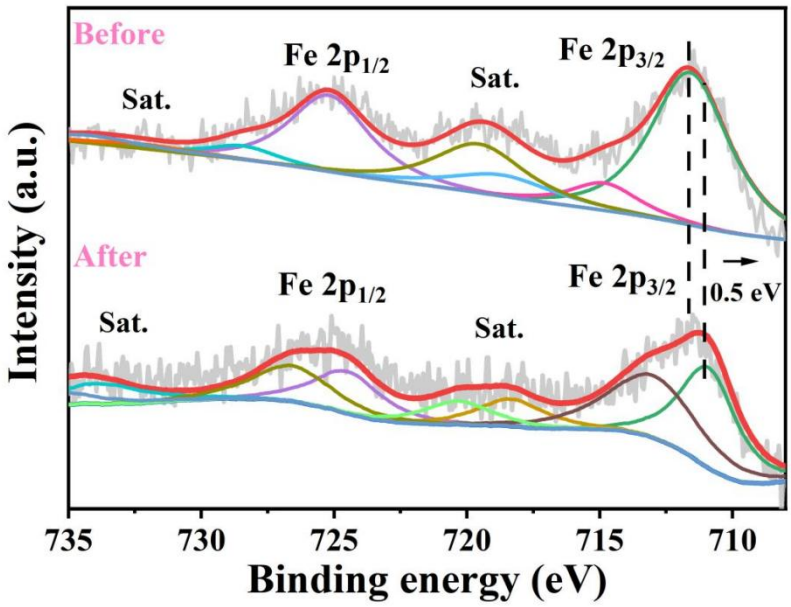

Fig. S13 High-resolution XPS spectra of Fe 2p after NO_3RR test.

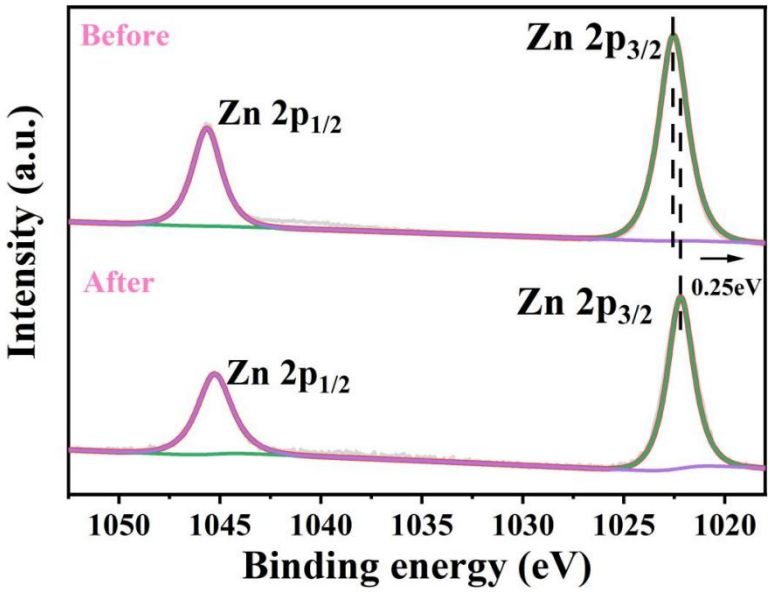

Fig. S14 High-resolution XPS spectra of Zn 2p after NO_3RR test.

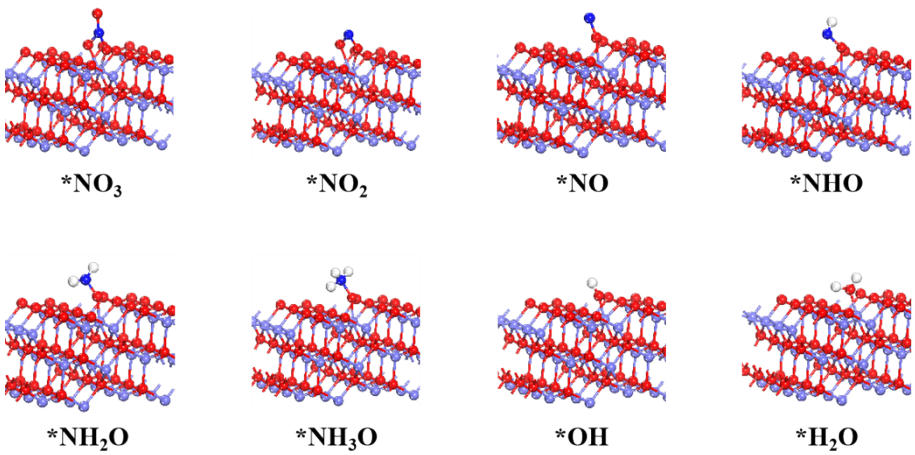

Fig. S15 The proposed reaction mechanism of nitrate electroreduction on the surface of ZnO.

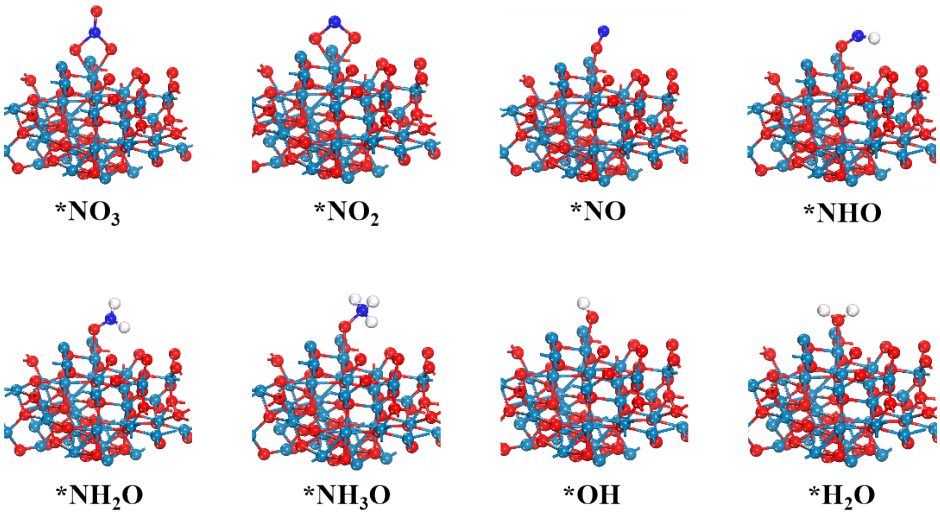

Fig. S16 The proposed reaction mechanism of nitrate electroreduction on the surface of Fe_2O_3.

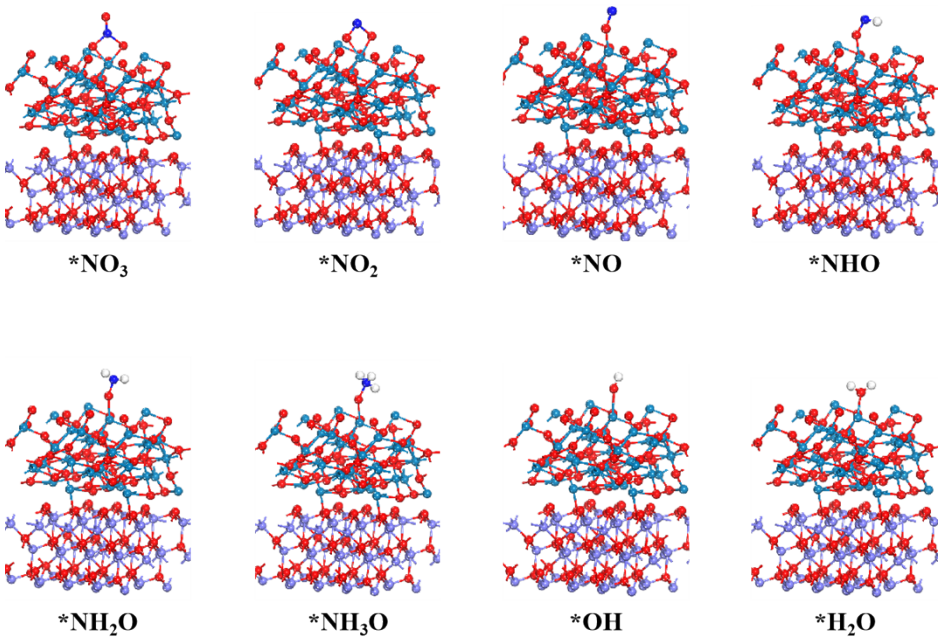

Fig. S17 The proposed reaction mechanism of nitrate electroreduction on the surface of Fe_2O_3/ZnO.

Table S1. The comparison of electrochemical ENO_3RR performance between Fe_2O_3/ZnO and some other reported electrocatalysts in neutral electrolytes.

Electrocatalysts	Electrolytes	Performance	Ref.
Fe_2O_3/ZnO	0.1 M KNO_3 0.1 M PBS	rNH_3: 0.37 mmol h^{-1} cm^{-2} (6.3 mg h^{-1} cm^{-2}) FE NH_3: 97.4% (-1.0 V vs. RHE)	**This work**
OD-Cu cubes	0.1 M KNO_3 0.1 M PBS	rNH_3: 0.22 mmol h^{-1} cm^{-2} FE NH_3: 93.9% (-0.9 V vs. RHE)	6
Co_2P	0.1 M $NaNO_3$ 0.5 M Na_2SO_4	rNH_3: 0.30 mmol h^{-1} cm^{-2} FE NH_3: 88.6% (-0.6 V vs. RHE)	7
PdCoO/NF	0.5 M PBS 200 ppm NO_3^-	rNH_3: 0.204 mmol h^{-1} cm^{-2} FE NH_3: 88.6% (-1.3 V vs. RHE)	8
FOSP-Cu-0.1	0.5 M Na_2SO_4 0.1 M KNO_3	rNH_3: 0.10 mmol h^{-1} cm^{-2} FE NH_3: 93.91% (-0.266 V vs. RHE)	9
Ni_1Fe_1	0.1 M Na_2SO_4 200 ppm NO_3^-	rNH_3: 0.216 mmol h^{-1} cm^{-2} FE NH_3: 74.8% (-0.75 V vs. RHE)	10
$Cu_{SA}NPC$	0.01 M PBS 500 mgL^{-1} NO_3^-	rNH_3: 0.153 mmol h^{-1} cm^{-2} FE NH_3: 87.2% (-1.1 V vs. RHE)	11
Co_3O_4/Co-h	0.1 M Na_2SO_4 1000 mgL^{-1} NO_3-	rNH_3: 0.26 mmol h^{-1} cm^{-2} FE NH_3: 88.7% (-0.8 V vs. RHE)	12

Fe SAC	0.1M K_2SO_4 0.5 M KNO_3	rNH_3: 0.46 mmol h^{-1} cm^{-2} FE NH_3: 74.9% (-0.66 V vs. RHE)	13
Cu/TiO_{2-x}	0.5 M Na_2SO_4 200 ppm NO_3^-	rNH_3: 0.11 mmol h^{-1} mg^{-1} FE NH_3: 81.3% (-0.75 V vs. RHE)	14
Cu-NBs-100	0.1 M PBS 500 ppm NO_3^-	rNH_3: 0.13 mmol h^{-1} cm^{-2} (-0.15 V vs. RHE)	15

Table S2. N_2 production of Fe_2O_3/ZnO at different potentials.

Potential (V)	**The yield of the produced N_2 (g)**
-1.411	0.812×10^{-3}
-1.511	0.644×10^{-3}
-1.611	0.448×10^{-3}
-1.711	0.532×10^{-3}
-1.811	0.700×10^{-3}

Table S3. The calculated reaction free energy for the elementary steps over three catalysts.

Elementary step	**ZnO**	**Fe_2O_3**	**Fe_2O_3/ZnO**
$*+NO_3\rightarrow*NO_3$	-0.43	-0.79	-1.16
$*NO_3\rightarrow*NO_2$	-0.63	-0.53	-0.80
$*NO_2\rightarrow*NO$	-2.14	-2.36	-2.58
$*NO\rightarrow*NHO$	0.95	0.68	0.47
$*NHO\rightarrow*NH_2O$	-0.34	-0.90	-0.70
$*NH_2O\rightarrow*NH_3O$	-1.42	-0.67	-0.57
$*NH_3O\rightarrow*OH$	-2.34	-1.29	-0.55

OH→H_2O	-0.36	-0.70	-0.50
H_2O→+H_2O	0.40	0.26	0.09

4. Reference

1. G. Kresse and J. Furthmüller, *Comput. Mater. Sci*. 1996, **6**, 15-50.
2. G. Kresse and J. Furthmüller, *Phys. Rev. B* 1996, **54**, 11169-11186.
3. J. P. Perdew, K. Burke and M. Ernzerhof, *Phys. Rev. Lett*. 1996, **77**, 3865-3868.
4. G. Kresse and D. Joubert, *Phys. Rev. B* 1999, **59**, 1758-1775.
5. P. E. Blöchl, *Phys. Rev. B* 1994, **50**, 17953-17979
6. N. Zhou, Z. Wang, N. Zhang, D. Bao, H. X. Zhong and X. B. Zhang, *ACS Catal.* 2023, ***13***, 7529-7537.
7. L. C. Yi, P. Shao and Z. H. Wen, *New J. Chem.* 2023, **47**, 9545-9549.
8. M. Liu, Q. Mao, K. Shi, Z. W. Qiang, X. You, N. L. Xiao, W. Liang and J. W. Hong, *ACS Appl. Mater. Interfaces* 2022, **14**, 13169-13176.
9. Y. L. Zhao, Y. Liu, Z. J. Zhang, Z. K. Mo, C. Y. Wang and S. Y. Gao, *Nano Energy* 2022, **97**, 107124.
10. W. Xuan, J. M. Ai, H. Jun, L. Dan, A. T. Kuvarega, B. B. Mamba and Z. G. Jian, *Inorg. Chem. Front.*, 2023, **10**, 666.
11. Y. Z. Xue, G. Qin, D. Fan, Z. Kun, C. Shuo, T. Y. Hong and Q. Xie, *Chem. Eng. J.*, 2023, **466**, 143314.
12. F. L. Zhao, G. T. Hai, X. Li, Z. Y. Jiang and H. H. Wang, *Chem. Eng. J.* 2023, **461,** 141960.
13. Z. Y. Wu, M. Karamad, X. Yong, Q. Huang, D. A. Cullen, P. Zhu, C. Xia, Q. Xiao, M. Shakouri, F. Y. Chen, J. Y. T. Kim, Y. Xia, K. Heck, Y. Hu, M. S. Wong, Q. Li, I. Gates, S. Siahrostami and H. Wang, *Nat.Commun.* 2021, **12**, 2870.
14. X. Zhang, C. H. Wang, Y. M. Guo, B. Zhang, Y. T. Wang and Y. F. Yu, *J. Mater. Chem. A* 2022, **10**, 6448-6453.
15. Q. Hu, Y. J. Qin, X. D. Wang, Z. Y. Wang, X. W. Huang, H. J. Zheng, K. R.

Gao, H. P. Yang, P. X. Zhang, M. H. Shao and C. X. He, *Energy Environ. Sci.* 2021, **14**, 4989-4997.